A Photoresponsive Red-Hair-Inspired Polydopamine-Based Copolymer for Hybrid Photocapacitive Sensors

Marianna Ambrico, Nicola Fyodor Della Vecchia, Paolo F. Ambrico, Antonio Cardone, Stefania R. Cicco, Teresa Ligonzo, Roberto Avolio, Alessandra Napolitano, and Marco d'Ischia**

Inspired by the powerful photosensitizing properties of the red hair pigments pheomelanins, a photoresponsive cysteine-containing variant of the adhesive biopolymer polydopamine (pDA) is developed via oxidative copolymerization of dopamine (DA) and 5-S-cysteinyldopamine (CDA) in variable ratios. Chemical and spectral analysis indicate the presence of benzothiazole/benzothiazine units akin to those of pheomelanins. p(DA/CDA) copolymers display impedance properties similar to those of biological materials and a marked photoimpedance response to light stimuli. The use of the p(DA/CDA) copolymer to implement a solution-processed hybrid photocapacitive/resistive metal-insulator-semiconductor (MIS) device disclosed herein is the first example of technological exploitation of photoactive, red-hair-inspired biomaterials as soft enhancement layer for silicon in an optoelectronic device. The bio-inspired materials described herein may provide the active component of new hybrid photocapacitive sensors with a chemically tunable response to visible light.

1. Introduction

The development of photo-capacitor-based optical sensors with a high dynamic range and wavelength (color)-discrimination capability is an important goal in current electronics due to their broad range of applications such as medical tomography, industrial monitoring system, surveillance system, computer vision system, scientific research applications, broadcasting system, and consumer appliances, hyperspectral imaging.[1] Device efficiency depends on the availability of photosensitive materials with a dielectric constant and a capacitance that change upon illumination with a high dynamic response and in a broad wavelength range.[2,3] Insertion of the device in a radiofrequency oscillator would thus allow to generate a wireless frequency-modulated signal in response to intensity modulation of incident light.[2,4,5] Several inorganic semiconductors, ranging from Si to GaAs, GaN and AlGaN, have been employed in meta-insulator-semiconductor (MIS), Schottky barrier or (p-type)-intrinsic-(n-type) (p-i-n) semiconductor-based conceived photocapacitors. In all cases, either depletion or metal-oxide-semiconductor (MOS) capacitance is changed upon illumination.[4–10] Despite satisfactory performances, however, inorganic photocapacitive detectors, like those based on Si, suffer from drawbacks relating to high costs and high environmental impact. An attractive alternative would be offered by soft, friendly and more easily processable organic semiconductors. Unfortunately, organic photocapacitive and photoresistive detectors generally show a low photo-efficiency, due to the narrow spectral responsiveness, and have been little investigated, with phthalocyanine-based systems being the most significant examples.[4–10] A possible convenient means of circumventing the intrinsic limitations of organic photocapacitors is to create a hybrid photosensitive device by coating a silicon substrate with a suitable organic film (such as a conjugated polymer) serving as an 'enhancement layer' for broadband UV-visible detection.[11,12] To fulfill this scope, the organic layer should exhibit a broadband spectral response, absorbing light at high energies where the silicon photo-response is poor, and should emit at longer wavelengths.[12] Improved photo-efficiency would thus results from both a higher UV absorption coefficient and a substantial emission at longer wavelengths of the organic polymer, providing the silicon with photons enhancing the opto-electrical response.

Among the various classes of organic semiconductors that can be considered as possible silicon enhancing layers, the melanins appear to be particularly attractive candidates. These

Dr. M. Ambrico, Dr. P. F. Ambrico
CNR-Istituto di Metodologie Inorganiche e dei Plasmi
Via Orabona 4, I-70125 Bari, Italy
E-mail: marianna.ambrico@cnr.it
Dr. N. F. D. Vecchia, Prof. A. Napolitano,
Prof. M. d'Ischia
University of Naples "Federico II"
Department of Chemical Sciences
Via Cintia 4, I-80126 Naples, Italy
E-mail: dischia@unina.it
Dr. A. Cardone, Dr. S. R. Cicco
CNR-Istituto di Chimica dei Composti Organo-Metallici-UOS di Bari
Via Orabona 4, I-70125 Bari, Italy
Prof. T. Ligonzo
Dipartimento Interateneo di Fisica
Università degli Studi di Bari "Aldo Moro"
Via Orabona 4, I-70125 Bari, Italy
Dr. R. Avolio
CNR – Institute of Chemistry and Technology of Polymers
Via Campi Flegrei 34, 80078 Pozzuoli, Italy

DOI: 10.1002/adfm.201401377

are complex and structurally heterogeneous phenolic pigments of different origin which are found in man and various organisms at all levels of the evolutionary scale and play a variety of biological roles.[13] Main classes of human melanin pigments comprise: a) the eumelanins, black-to-brown insoluble pigments resulting from the oxidative polymerization of L-dopa via 5,6-dihydroxyindole (DHI) intermediates; and b) the pheomelanins, yellow-to-reddish brown pigments resulting from the oxidative conjugation of dopa and cysteine to give cysteinyldopa precursors, mainly 5-S-cysteinyldopa, which polymerize via benzothiazine and benzothiazole intermediates. While eumelanins are supposed to be photoprotective due to a broadband absorption throughout the entire UV-visible range, structure-dependent free radical properties and efficient UV dissipation properties,[14] pheomelanins display marked photosensitizing properties, which are commonly implicated in the familiar susceptibility of red-haired fair-skinned individuals to sunburn and skin cancer.[14,15] Following the demonstration that eumelanins behave as unique hybrid electronic-ionic conductors,[16] considerable interest has been directed to investigate the potential of eumelanin-type materials for exploitation in organic electronics, e.g. in light emitting diodes and field effect transistors.[16–21]

Recently, we demonstrated that polydopamine (pDA) (or dopamine-melanin), a versatile eumelanin-type polymer with strong adhesion properties,[22–26] displays semiconductor-like properties that can be modified by chemical manipulation. In particular, covalent incorporation of aromatic amines into the pDA structure during polymerization induced a marked shift of the flat band voltage tuning its intrinsic semiconductor properties to n-type behavior.[27] Considerable interest was therefore raised in this context by the possibility of using pDA as a silicon enhancing layer in hybrid photo-capacitive sensors.[2,4,5] Use of pDA as the photoactive matrix was envisaged to offer better opportunities compared to other melanins for the superior adhesion and processability properties, coupled with an intense absorption in the UV region.[22,26,28–31] Moreover, the high dielectric constant makes pDA/Si structure a valuable alternative to SiO_2/Si or similar photocapacitive structures. The impedance frequency dispersion spectra also suggests that melanin-based photocapacitors could use the alternate current (AC) signal frequency to modulate the device sensitivity and the dynamic range.[27] In principle, a critical drawback in the application of pDA, and more in general of eumelanins, for photosensitive devices is related to non-radiative excited state decay associated with poor emission properties despite a high extinction coefficient in the UV range.[14] It was envisaged, however, that this limitation could be circumvented by chemical manipulation of the pDA structure. It is worth mentioning in this regard a paper reporting insertion of a p-doped pDA thin film with a dense and conformal surface as an optically active channel in OTFT transistors to implement an organic phototransistor with high photosensitivity and photo-controlled switching properties.[21]

An attractive bio-inspired strategy to improve the light response of pDA is based on the incorporation within the pDA scaffold of pheomelanin-type benzothiazine and benzothiazole units that could serve as photosensitizing components. Although pheomelanins exhibit intrinsically poor emission properties with a complex dependence of quantum yields on the excitation energy, they can easily eject electrons upon photoexcitation, as evidenced by free electron laser-photoelectron emission microscopy.[32] The use of pheomelanin-like materials for technological purposes is entirely unprecedented and was envisaged to offer valuable opportunities to enhance the electrical properties of the Si substrate.[32,33] Prompted by the above considerations, we report in this paper the synthesis and characterization of poly(dopamine/5-S-cysteinyldopamine) (p(DA/CDA)) as a new material incorporating photosensitizing pheomelanin-related units into a eumelanin-type skeleton to enhance the light response of the polymer. Combining the features of the two main classes of human pigments, eumelanins and pheomelaninsm, is an innovative approach in materials science and a new entry to pDA modification, which differs profoundly from the previously reported strategy, involving polymerization of DA in the presence of aromatic amines as modifiers of π-electron properties.[27] In the present study, pheomelanin-type units are incorporated into the pDA system via copolymerization with CDA, a product of DA metabolism[34] resembling the pheomelanin precursor 5-S-cysteinyldopa but replacing the alanyl side chain with an ethylamine side chain on the catechol ring. Use of CDA rather than 5-S-cysteinyldopa was motivated by the closer similarity to DA preventing an unnecessary increase in the number of functional groups in the copolymerization products.

2. Results and Discussion

2.1. Characterization of p(DA/CDA)

The structural investigation of melanin-type materials is a notoriously difficult task which is usually carried out by combining spectral techniques and chemical degradation methodologies.[15] Recent studies have succeeded in characterizing the fundamental structural properties of pDA, revealing the presence in the material of uncyclized catecholamine units and cyclized 5,6-dihydroxyindole building blocks, together with pyrrolecarboxylic acid components.[28–31] Likewise, the nature of the species produced by oxidation of CDA was elucidated in early reports[34–36] showing the formation of 1,4-benzothiazine and benzothiazole structures arising from a chemical route similar to that described in the conversion of 5-S-cysteinyldopa to pheomelanin pigments (**Figure 1**).[37]

For the purposes of this study, pDA and pCDA were prepared by autoxidation of 10 mM catecholamine in 0.05 M NH_3 buffer, pH 8.5, while p(DA/CDA) samples were synthesized by co-oxidation of DA and CDA at 10 mM overall concentration under the same conditions. All samples were characterized by combining spectral techniques with an established chemical degradation methodology.[15] Analysis of the UV-visible spectra of the mixed p(DA/CDA) copolymers in comparison with those of pDA and pCDA (**Figure 2**) revealed significant differences. The pDA spectrum (trace a) showed as distinguishing feature an intense band at ca. 280 nm, attributed to uncyclized catecholamine units,[29] with very modest shoulders around 420 nm. On the other hand, the UV-visible spectrum of pCDA (trace d) proved similar to that of 5-S-cysteinyldopa pheomelanin, displaying a shoulder around 305 nm and a broad band below

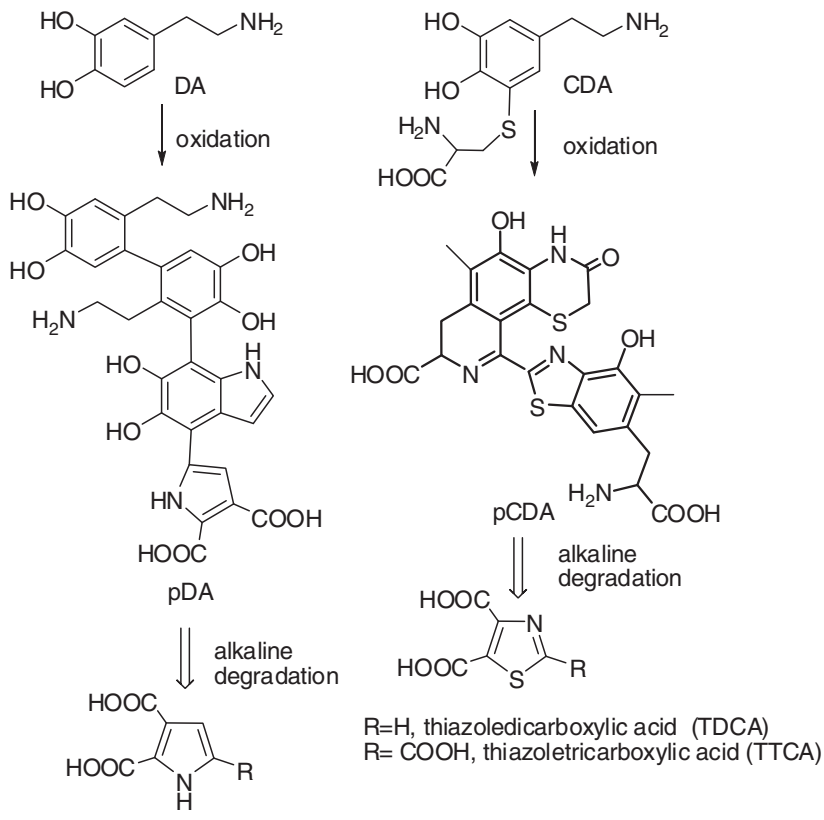

Figure 1. Structures of dopamine and 5-S-cysteinyldopamine, representative structural component of pDA and main structural units in pCDA (A, benzothiazine units, B, benzothiazole units), and standard eumelanin-pheomelanin structural markers.

400 nm, which can be attributed to benzothiazole and 2,2'–bi(benzothiazine) units, respectively.[38]

Inspection of the spectra of p(DA/CDA) samples (traces b and c) indicated in both cases the almost complete loss of the intense pDA UV band at ca. 280 nm, replaced by modest shoulders at slightly shorter wavelengths, and a significant absorption enhancement throughout the entire visible region with respect to pDA and pCDA traces, due in part to a very broad and flat band around 400 nm. The relative visible absorption properties of the materials can thus be conveniently expressed in terms of A_{400}/A_{280} absorbance ratios, which gave values of about 0.33 for pDA, 0.66 for pCDA, and 0.73 for both p(DA/CDA) samples.

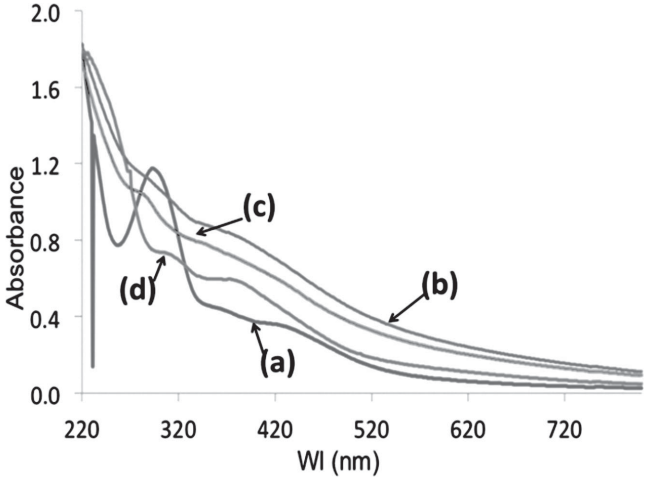

Figure 2. a) UV visible spectra of pDA, mixed type copolymers with b) 25% and c) 50% cysteinyldopamine, and d) pCDA. Spectra were taken from oxidation mixtures at 8 hrs reaction time following 1:50 v/v dilution in water.

The FTIR spectra of pDA, pCDA and the mixed p(DA/CDA) materials, recorded in the attenuated total reflectance (ATR) mode, are shown in **Figure 3**. The spectrum of pDA exhibited, besides an ammonium band at 1403 cm^{-1},[26] a rather broad band in the range between 1550–1600 cm^{-1} attributed to aromatic C = C and C = N stretching.[39] The spectrum of pCDA exhibited a characteristic series of bands in the region between 1450 and 800 cm^{-1} similar to those reported for synthetic pheomelanins from cysteinyldopa.[40] It is tempting to assign the band at 1450 cm^{-1}, which is missing in the pDA spectrum, to benzothiazole units, since the parent heterocycle gives two close bands in the range between 1500–1400 cm^{-1} (see Figure S2) Inspection of the p(DA/CDA) spectra revealed features that were attributable to a prevalent pDA component obscuring seemingly pCDA contributions. In one sample, a few very weak bands could be identified as possible signatures of distinctive structural components (Figure 3, trace c) but their assignment is not straightforward based on current data

The nature of the species contributing to p(DA/CDA) composition was also investigated by straightforward ^{13}C CP-MAS NMR analysis in comparison with pDA (**Figure 4**). The spectrum of p(DA/CDA) (panel B) exhibits as expected the typical features of pDA (panel A), namely intense aliphatic resonances around δ 30 and 40, and sp^2 carbon bands in the range between δ 110 and 150, suggesting the coexistence of uncyclized (dopamine-like) and cyclized (indolic) elements, as reported previously.[28] Major differences concern a more complex aromatic region in the case of p(DA/CDA), due evidently to the superposition of different signals, with intense contributions around δ 135 and 165. While the former band, which is missing in pDA, can be reasonably attributed to aromatic signals belonging to benzothiazine and benzothiazole units, the latter is typical of amide-type carbons in benzothiazinone moieties and of C2 carbons in 2-substituted benzothiazole rings, as recently reported[41] (see representative pCDA structural components in Figure 1). Carboxylic functions are likely to contribute to the low field inflection of the band at δ 170. It is worth noting that during pheomelanin synthesis a substantial proportion of cysteinyl carboxylate groups are usually lost following cyclization.[41]

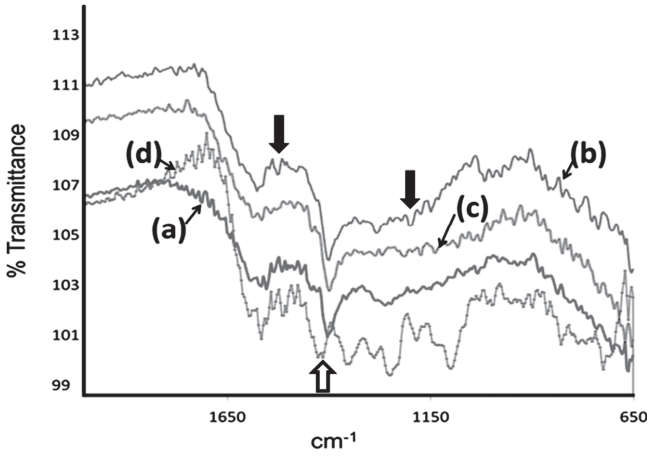

Figure 3. a) FTIR spectra of pDA mixed type copolymers with b) 25% and c) 50% cysteinyldopamine, and of d) pCDA. Spectra were recorded on solid samples in the attenuated total reflectance (ATR) mode. A possible benzothiazole band is shown by the empty arrow, while distinctive bands of the mixed melanins are indicated by black solid arrows.

Finally, all copolymers were analyzed by a state-of-the-art chemical degradation methodology for melanin characterization, which is based on alkaline hydrogen peroxide degradation followed by HPLC quantification of four specific markers:[15] a) pyrroledicarboxylic acid (PDCA), derived from unsubstituted pyrrole moieties; b) pyrroletricarboxylic acid (PTCA), an index of polymerized 5,6-dihydroxyindole units; c) thiazoledicarboxylic acid (TDCA), and 4) thiazoletricarboxylic acid (TTCA), both markers of pheomelanin-type benzothiazine/benzothiazole units.[36] It should be noted that the chemical degradation procedure does not allow to distinguish benzothiazine units and benzothiazole units, which derive from irreversible rearrangement of the former.

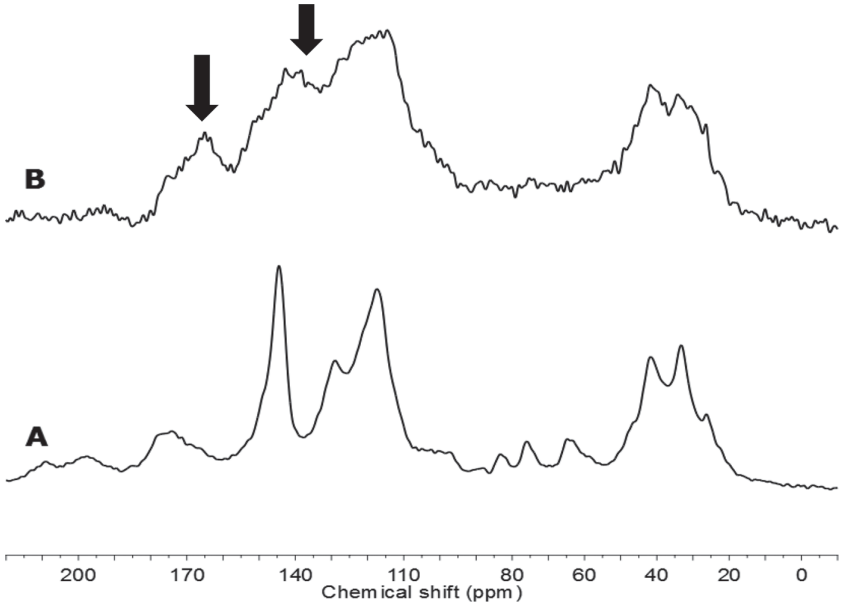

Figure 4. ^{13}C CP-MAS NMR spectra of A) pDA and B) p(DA/CDA) solid samples (neat). Black arrows in panel B denote characteristic signals of benzothiazine-benzothiazole units.

Table 1. Formation yields of chemical markers of eumelanin (PDCA and PTCA) and pheomelanin (TDCA and TTCA) in pDA, pCDA and mixed polymers.

Sample	Yield (± SD)% w/w			
	PTCA	PDCA	TTCA	TDCA
pCDA	—	0.718 ± 0,058	7.409 ± 0.282	0.326 ± 0.085
p(DA/CDA) 50:50	0.057± 0.019	0.599 ± 0.049	4.330 ± 0.423	0.337 ± 0.131
p(DA/CDA) 75:25	0.077 ± 0.028	0.457 ± 0.114	3.015 ± 0.063	0.470 ± 0.134
pDA	0.052 ± 0.003	0.503 ± 0.050	—	—

The results of chemical degradation experiments are shown in **Table 1**. From these data it can be concluded that p(DA/CDA) copolymers contain CDA-derived benzothiazine and benzothiazole units within the pDA backbone, as evidenced by the formation of both pheomelanin markers TTCA and TDCA. Although TTCA and TDCA are usually regarded as a reliable indices of pheomelanin levels in mixed samples, their use to determine the composition of mixed melanins may be subject to caveat due to the intrinsic limitations of the harsh degradation methodology when applied to a quantitative determination.[15] The formation of the eumelanin marker PDCA from pCDA suggested cyclization of the aminoethyl chain of CDA, as already observed in a previous study,[36] but it was not possible to estimate the extent of cyclization based solely on the small yields of PDCA. We have recently demonstrated[29] high proportions of uncyclized amine-containing units in pDA samples giving PDCA and PTCA yields similar to those of the present copolymers, whereby it seems likely that both pCDA and its copolymers retain a significant amount of amine-containing uncyclized units. Overall, the spectral and chemical characterization data reported herein unambiguously demonstrate the presence of pheomelanin units in the mixed polymers, thus providing the necessary chemical background to investigate the photocapacitive properties of the new mixed materials.[35,36]

2.2. pDA, p(DA/CDA), pCDA-Based Devices Testing

2.2.1. MIM Devices Results

Due to their DA-related basic units, bio-inspired p(DA/CDA) materials bear structural resemblance to the neuromelanin pigment of human Substantia Nigra and can be considered as biological–like items.[36,42] The impedance vs. frequency *(Z vs. f)* spectra readouts and subsequent extraction of the real (ε') and imaginary (ε'') part of permittivity and loss factor tan $\delta = \varepsilon'/\varepsilon''$ are sensitive methods to discriminate if a medium behaves like a biological or as a (poly)electrolyte material, because of the well known typical features of the impedance spectra of biological media (see S.I. and Figure S3).[43–45] The commonly

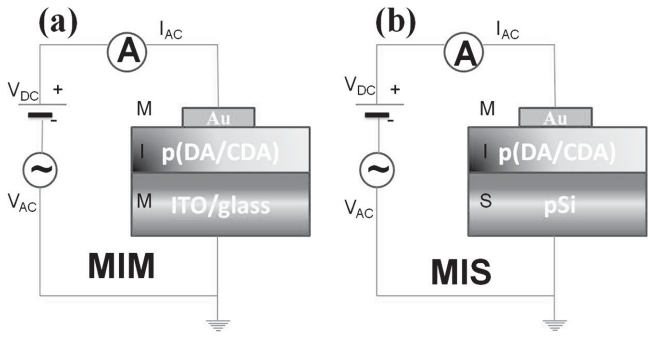

Figure 5. Simplified scheme representing a) left, the p(DA/CDA)-based MIM (on ITO/glass) and b) right, the p(DA/CDA)-based MIS on pSi devices.

adopted circuit configuration (**Figure 5**a) suitable for measuring the Z vs. f spectra and the dispersion of the real and imaginary parts of the dielectric permittivity is the metal – insulator – metal (MIM) one. This structure is realized by sandwiching the polymer layer (the "insulator") between a top metallic electrode (in our case gold, Au) and a glass support covered by a conducting indium tin oxide (ITO) film (i.e. ITO-glass) constituting the bottom electrode (see also details in the Experimental Section).

Figure 6 compares the in air real (ε') part of permittivities (6a) as extracted from the impedance spectra readouts obtained on p(DA/CDA) and on the pure pDA, pCDA-based MIM devices. Data representing the imaginary (ε'') part are shown in S.I. A strikingly different behavior was observed between copolymers and pure ones. It is noteworthy to observe that with respect to pDA and pCDA, in p(DA/CDA) copolymers the occurrence of a β-region indicates the similarity of the mixed polymer AC signal response to that of a biological item.[43,44] In pDA and pCDA pure polymers, the α relaxation region is the only one evidenced while the corresponding feature due to the double layer formation is shifted to a frequency lower than 10 Hz (data not shown). The mixed copolymer permittivity vs. frequency trend is furthermore similar to that observed in those of commercial synthetic melanin (SM). Relevant to note, the magnitude of the real permittivity was found one order higher than that of commercial SM layers. The inspection of the loss factor behavior vs. frequency *(tan δ vs. f)*, as derived from permittivity results, showed (Figure 6b) a β related loss peak furthermore occurring at the same frequency for both p(DA/CDA) and SM layers. The large increase of the loss factor at low frequency in the copolymers demonstrates the increasing of the AC conductivity.[45]

Figure 6(c–e) summarizes the capacitance behavior at three different frequencies (10 kHz, 1kHz and 100 Hz) of the AC voltage signal of p(DA/CDA) 75:25 (c) and 50:50 (d) and pCDA (e) based MIM devices under the on/off of a continuous white light source. No detectable response to white light illumination was observed in pDA-based MIM devices at all the AC voltage signal frequencies (data not shown). On the other hand, the response of pCDA-based MIM devices to white light started at around 10 kHz, and was particularly pronounced with an oscillating behavior at 1.0 kHz and 100 Hz. Such results evidenced the CDA promoted photo-generation of charges able to be coupled from 100 Hz up to a 10 kHz signal frequency and resulting in a peculiar light induced oscillating behavior of the polymer photoimpedance.

2.2.2. MIS Devices Results

In Air: The impedance spectroscopy characterization performed on pDA, pCDA and p(DA/CDA) -based MIM devices was suitable for evidencing the dielectric response in dark and under white light of the polymers layers. The MIS device configuration on pSi with pDA, pCDA and p(DA/CDA) as 'insulating' and optically active layers was instead adopted in order to check the MIS photocapacitive effect when the device is exposed to white light under depletion conditions.[6–9]

The **Figure 7** compares the C-V (7a) and G-V (7b) hysteresis loops read outs at 1 MHZ of the full set of pDA and p(DA/CDA)-based MIS devices collected in dark. The selected high frequency of the AC voltage signal allowed to avoid any influence of the interface state charges on the measured impedance.[46] The results showed the well known C-V hysteretic behavior in pDA-based structures, somewhat decreased in mixed p(DA/CDA) structures.[19,27] The loop direction was clearly detectable in pDA and p(DA/CDA) 75:25-based MIS devices, thus confirming the hole trapping mechanisms observed in similar pDA-based MIS structures on pSi.[27] The flat band capacitance and conductance relative variations respect to pDA insulating layer, (Figure 7c), increased by one order of magnitude with the addition of the CDA component. The flat band voltage was left shifted i.e. it increased (Figure 7a) with the pCDA proportion and suggested, together with the observed increase in AC conductance, a 'doping effect' (Fermi level shift) similar to that previously reported.[27]

Figure 8 summarizes the C-V read out at different frequencies in the dark (Figure 8a, c, e, and g) and under white light (WL, Figure 8b, d, f, and h). In the dark and at the flat band voltage, the capacitance increased with decreasing the frequency of the AC signal. This effect was a consequence of the dielectric constant frequency dispersion of the pDA and p(DA/CDA) insulating layers (see also Figure 6a). At the lowest frequency and under depletion conditions (0V ÷ +3V), no charge inversion layer was detected. This behavior suggested a lower 'doping efficiency' of pCDA with respect to the recently described pDA manipulation by aromatic amines (for example by *p*-phenylenediamine).[27] In the present case, the flat band voltage value indicated that a higher threshold voltage is required to induce the formation (at low AC frequency) of the charge inversion layer at the interface able to compensate the accumulaton capacitance.[46]

The pDA and p(DA/CDA) -based MIS devices showed a pronounced sensitivity to white light illumination (see Figure 8b, d, f, and h). Notably, the curves collected on p(DA/CDA)-based MIS structures at the higher frequencies, i.e. 100 kHz and 1 MHz, showed a marked photo-induced bump in the depletion region (0 V ÷ 3.0 V). This indicated a fast build up of a photo-induced capacitance, although the photocarrier density was not sufficient to compensate that the accumulation capacitance. Such a compensation occurred in the p(DA/CDA)-based devices at an interestingly high frequency value (f = 10 kHz, Figure 8f, h).

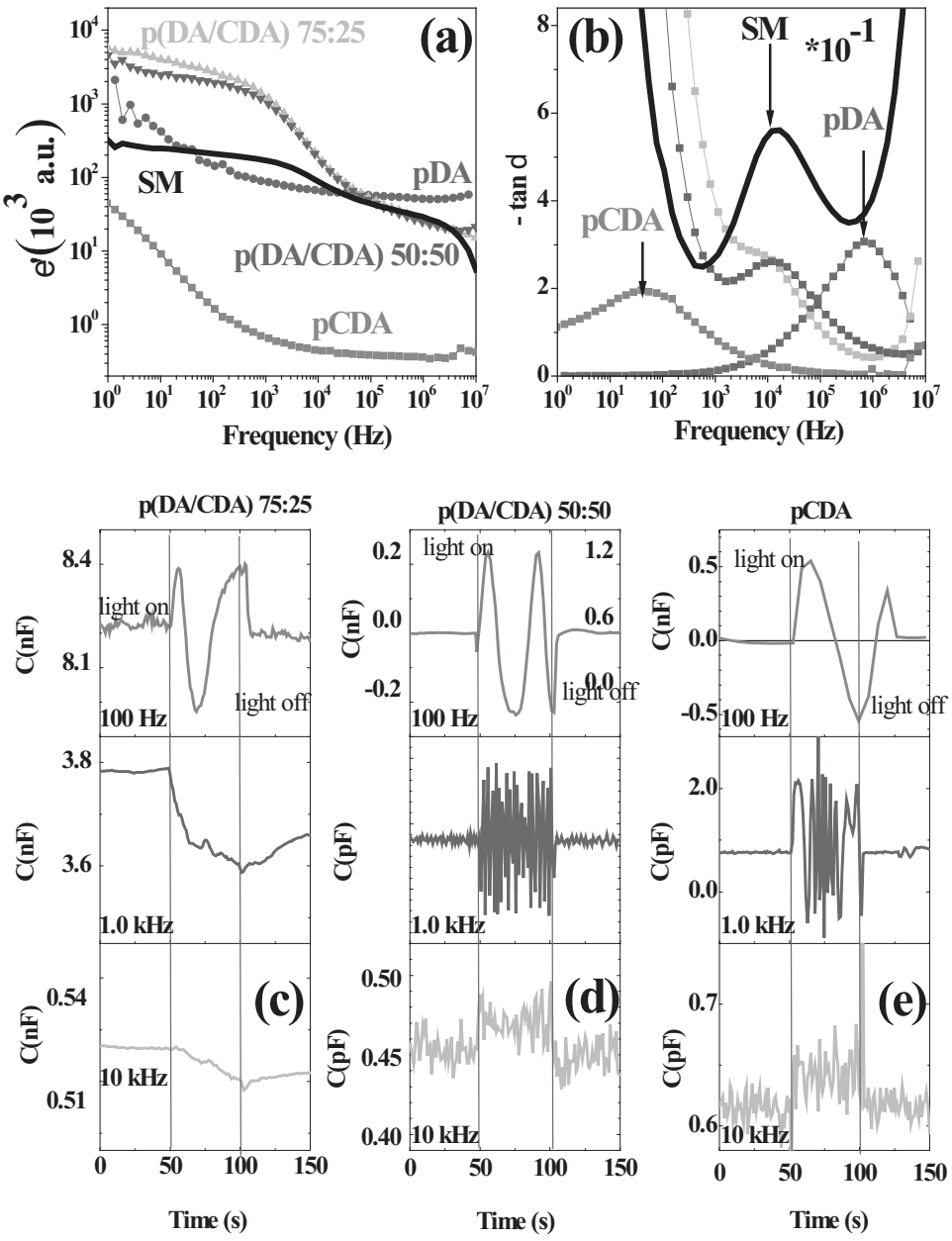

Figure 6. a) Real (ε') part of the layer permittivity as determined from *Z vs. f* measurements on a 400 nm thick pDA, p(DA/CDA) 75:25, p(DA/CDA) 50:50 layer-based MIM devices. Similar data from a 400 nm SM-based MIM device have been shown for comparison. b) Loss factors *tan δ vs. f* from data in Figure 6a and Figure S4. c-e) Photo-capacitance on-off taken at zero DC bias and at frequencies of 10 kHz, 1.0 kHz and 100 Hz of the AC voltage signals on p(DA/CDA) 75:25 (c) and 50:50 (d) and pCDA (e) based MIM devices.

To gain a deeper insight into the observed phenomena, the photo-assisted capacitance effects were examined at different frequency of the AC voltage signals and the photo-capacitance yields were compared. As an example, the readouts on the full set of MIS devices at f = 1.0 kHz are shown in **Figure 9**a. The results evidenced that mixed p(DA/CDA) 50:50-based MIS structures posses the highest photo-capacitance yield that combines with a photo-carrier charge density able to follow a high frequency signal. In order to quantitatively evaluate the photo-capacitive response, the yield was calculated by using the results from light-induced on-off of the photo-capacitance (Figure S6) whne applying the same AC voltage signal frequencies and biasing the MIS device under the depletion condition (V_{DC} = +2.5 V, see Figure S8 in S.I.). It is noteworthy that, on the whole, the pDA and pCDA -based MIS device displayed the lowest photo-capacitance yield in the overall frequency range of the AC voltage signal (Figure 9b). However, in pDA-based devices the higher yield was at the low frequency, while it was slightly increasing at high frequency in pCDA ones. Interestingly, in the structures made by p(DA/CDA) copolymers the higher the AC voltage signal frequency the higher the photo-capacitance yield was. Specifically, the 75:25-based

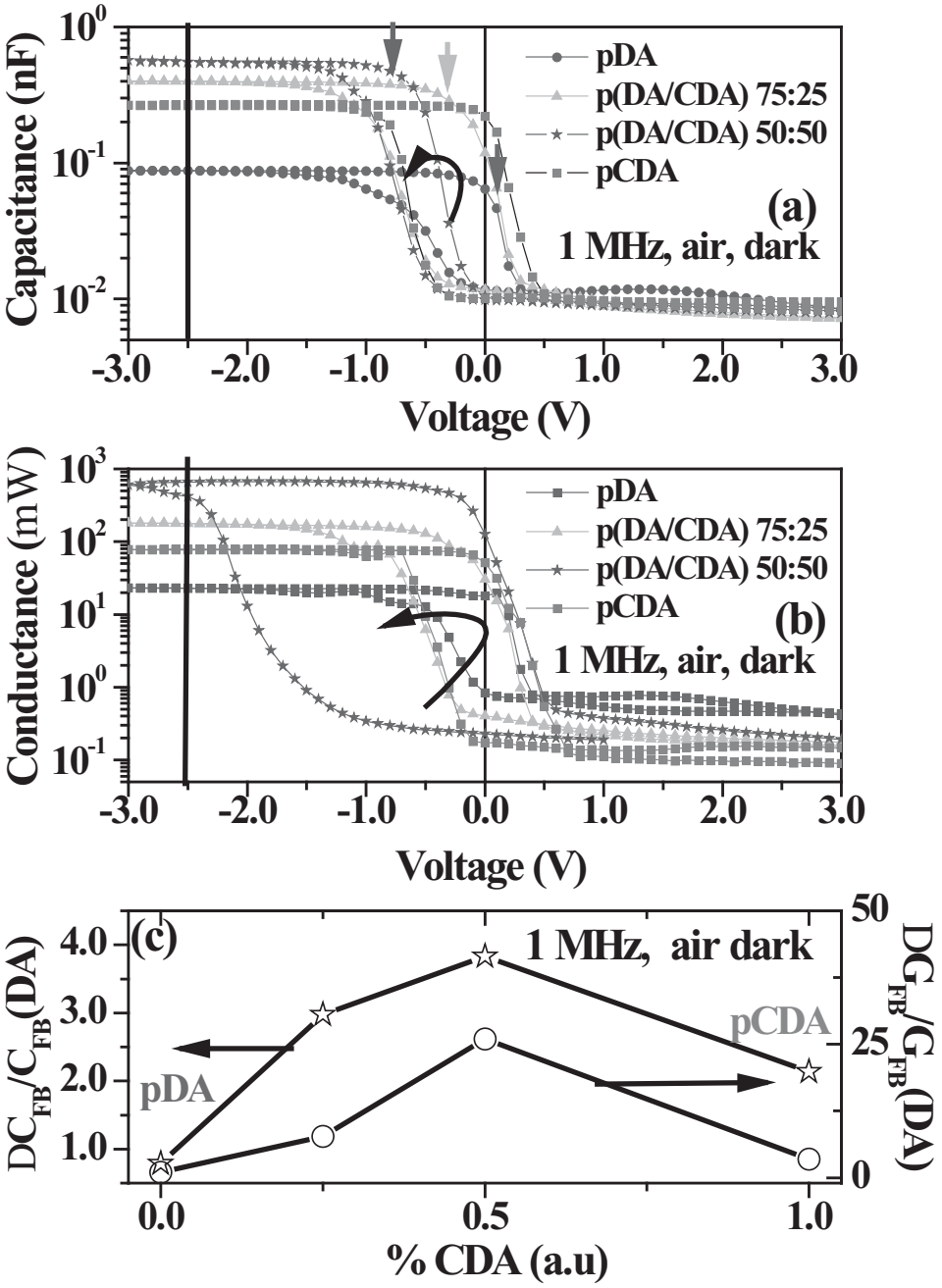

Figure 7. In air a) C-V and b) G-V hysteresis loops collected at 1.0 MHz on pDA, p(DA/CDA) and pCDA based MIS devices. The arrows in (a) indicate the flat band voltage V_{FB} values increasing with the pCDA content. The curved arrows represents the hysteresis loop rotation. The vertical lines indicate the value (V = – 2.5 V) of the voltage in the flat band region of the accumulation MIS regime where the band capacitances C_{FB} in (a) and conductances G_{FB} (b) have been taken. The C_{FB} and G_{FB} of the pDA-based MIS device are used as the reference values for the estimate of the relative variation of the flat band capacitance. c) Relative variation of the flat band capacitance $\Delta C_{FB}/C_{FB}(DA)$ (left, stars), $\Delta C_{FB} = C_{FB}(pDA/DA) - C_{FB}(pDA)$, and conductance $\Delta G_{FB}/G_{FB}(DA)$ (right, circles), $\Delta G_{FB} = G_{FB}(pDA/DA) - G_{FB}(pDA)$, *vs.* pCDA percentage.

and 50:50-based p(DA/CDA) structures display a noticeable yield increase up to 10 kHz and 1.0 kHz, respectively. This was explained as being due to a combined effect of the pCDA-driven yield enhancement towards the high signal frequency and of the higher optical absorption cross-section observed in mixed polymer-based structure.

In Vacuo: In vacuo and in the dark, the C-V read outs for pDA and pCDA-based MIS devices revealed the well known reversal of the hysteretic loop direction (see Figure S5 a,c,e,g in S.I.) besides to the expected absence of the dependence on frequency of flat band capacitance due to the water desorption and removal of water related interface states. This

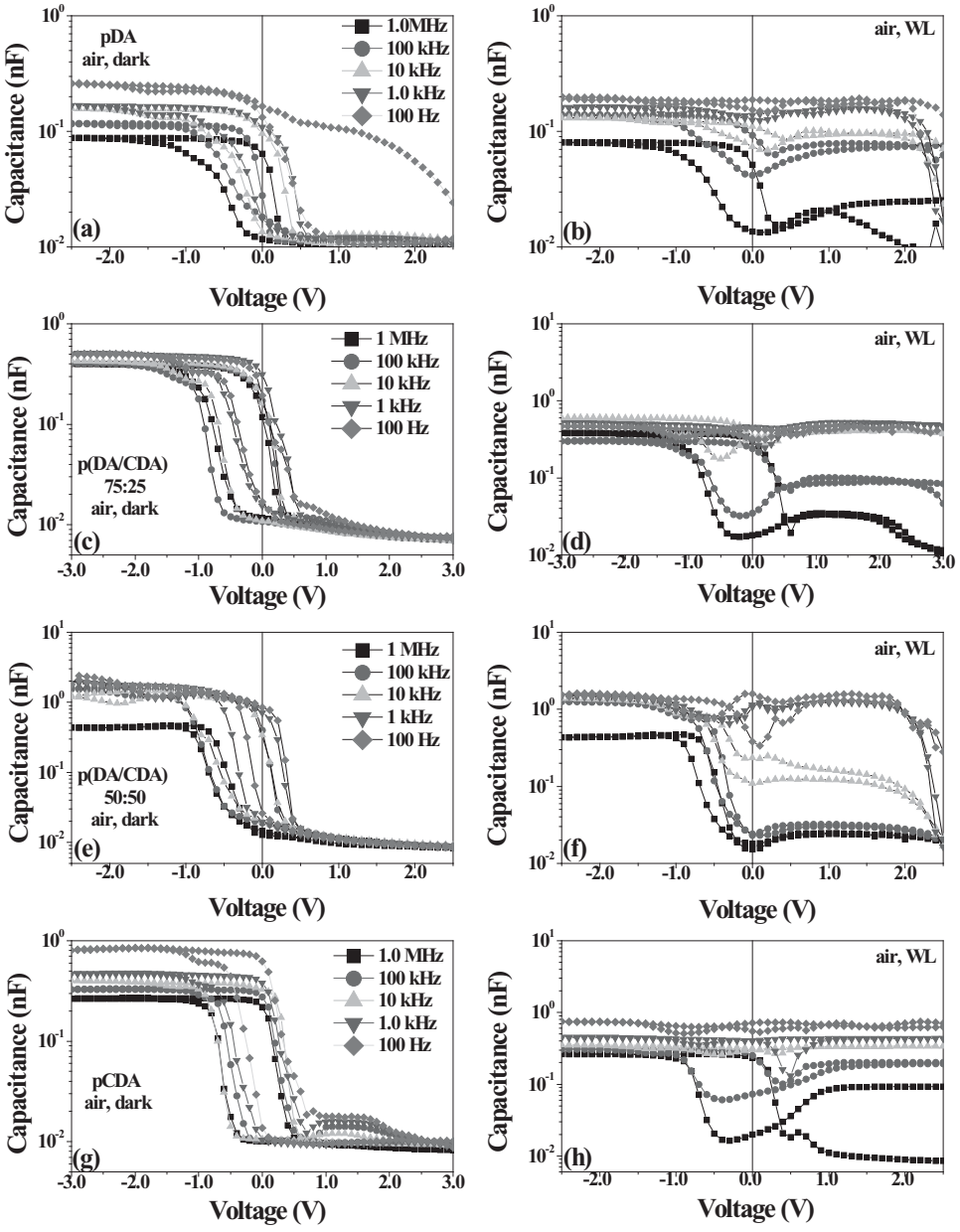

Figure 8. In air, C-V hysteresis loops at different frequency of the AC voltage on pDA and p(CDA/DA)-based MIS devices in the dark (left column) and corresponding loops under white light (right column).

behavior was also kept in structures including the mixed polymers with the lowest CDA content. No reversal of the hysteresis loop direction was detected in p(DA/CDA) 50:50 –based structures while keeping a behavior similar to that observed in air. By comparing C-V and G-V loops (**Figure 10**), a valuable increase of the flat band capacitance (10a) and conductance (10b) values was encountered, similar to that observed in air. This result evidenced that the observed doping effect was not due to hydration. The relative variation as a function of the pCDA content of the flat band capacitance (left, stars) and conductance (right, circles) of the p(DA/CDA)-based MIS devices normalized to that of pDA-based MIS one were summarized in Figure 10d.

With respect to ambient air measurements, an evident rightward shift was detected in flat band voltage of pCDA and p(DA/CDA)-based MIS devices (see arrows in Figure 10a). Moreover, the higher the CDA content the higher the flat band voltage displacement. The results were straightforward, considering that in melanin-based polymers the displacement of ionic charge leading to a dipolar contribution can be better evidenced in a vacuum. This because, in ambient air, water-mediated transport via charge (electrons or holes) hopping mechanisms overwhelm that of dipole one.[47] The flat band voltage rightward shift in the pCDA-based MIS devices, with respect to pDA-based ones, also suggested the presence of a dipole on the pSi surface, as represented in the sketch of Figure 10c.

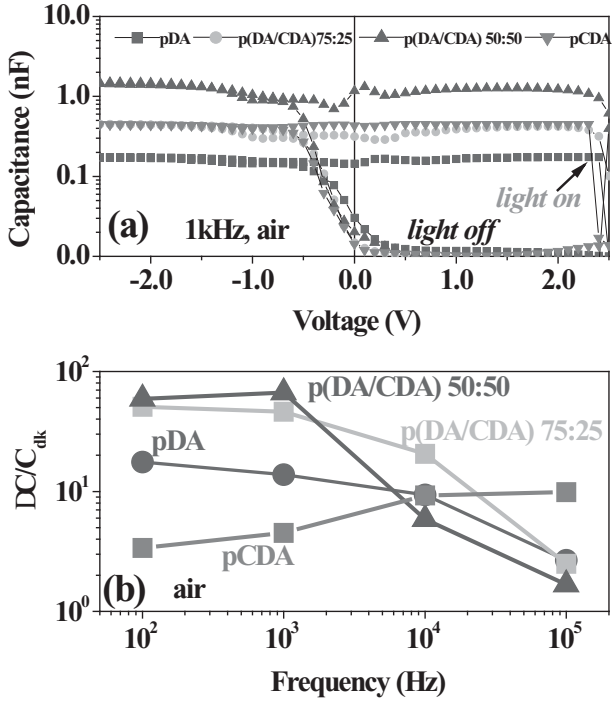

Figure 9. In air: a) Typical photo-assisted C-V data collected at 1 kHz on pDA, pCDA and p(DA/CDA)-based MIS devices. The light was switched on at a voltage V = + 2.5 V under MIS depletion condition. (b) Photocapacitance yield $\Delta C/C_{dk}$ as resulting from photo-assisted C-V measurements at different frequencies of the AC signal.

Figure 11 summarizes representative photo-capacitance results at 1.0 kHz (11a) and the extracted photo-yield behaviour under white light and at the different AC signal frequencies (11b) Again, the best efficiency was inferred in structures embodying the mixed polymer although in p(DA/CDA) 50:50-based MIS devices the photo-capacitance effect starts at + 1.0 V. It is noteworthy that, with respect to pDA-based devices, the structures with pCDA and p(DA/CDA) 75:25 layers showed an increase in the photo-capacitance yield of one order of magnitude while keeping it nearly constant throughout the entire signal frequency range up to 1.0 MHz. In pDA-based devices, a reduction of photo-efficiency was observed at low frequency. These results can be explained because, in the dark, the low frequency signal already induce a charge inversion layer under MIS depletion, partially compensating the flat band accumulation capacitance (see Figure S5a)

3. Mechanism of pCDA-Enhanced pDA Photoresponse

Polymerization of CDA or copolymerization with DA leads to heterogeneous disordered materials with pheomelanin-type benzothiazole and benzothiazine units, which exert a dual effect on the eumelanin backbone of pDA. In the dark, CDA-related units can account for a modest doping effect, which does not compare with that of aromatic amines.[27] This can be attributed to the possible occurrence of benzothiazine units in different oxidation states, ranging from the oxidized o-quinoneimine

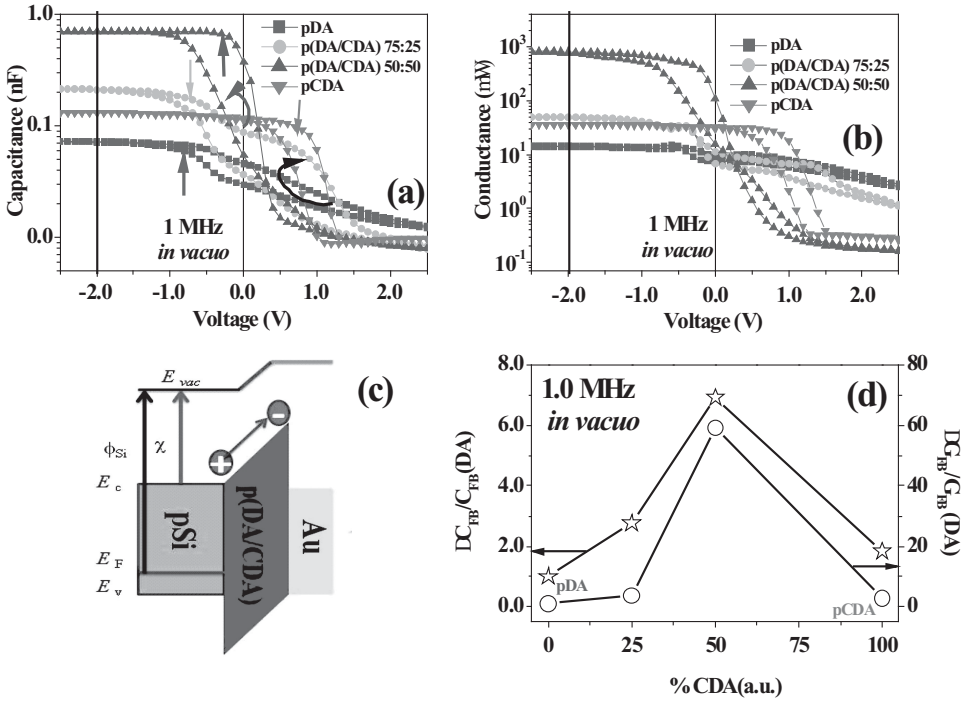

Figure 10. In vacuo: a) C-V and b) G-V hysteresis loops collected at 1 MHz on pDA, p(DA/CDA) and pCDA based MIS devices. The arrows in (a) indicates the flat band voltage V_{FB} values right shifting with the pCDA content. The curved arrows represents the hysteresis loop rotation. The black line indicates the value (V = –2.5 V) of the voltage in the flat band region of the accumulation MIS regime where the band capacitances C_{FB} in (a) and conductances G_{FB} (b) have been taken. c) Relative variation of the flat band capacitance $\Delta C_{FB}/C_{FB}$(DA) (left, stars) and conductance $\Delta G_{FB}/G_{FB}$(DA) (right, circles) variation *vs.* pCDA content. The meaning of ΔC_{FB} and ΔG_{FB} are the same of Figure 7. d) Simplified sketch of energetic band diagram as deduced from the flat band voltage right shift observed in in vacuo C-V data and attributed to surface dipole.

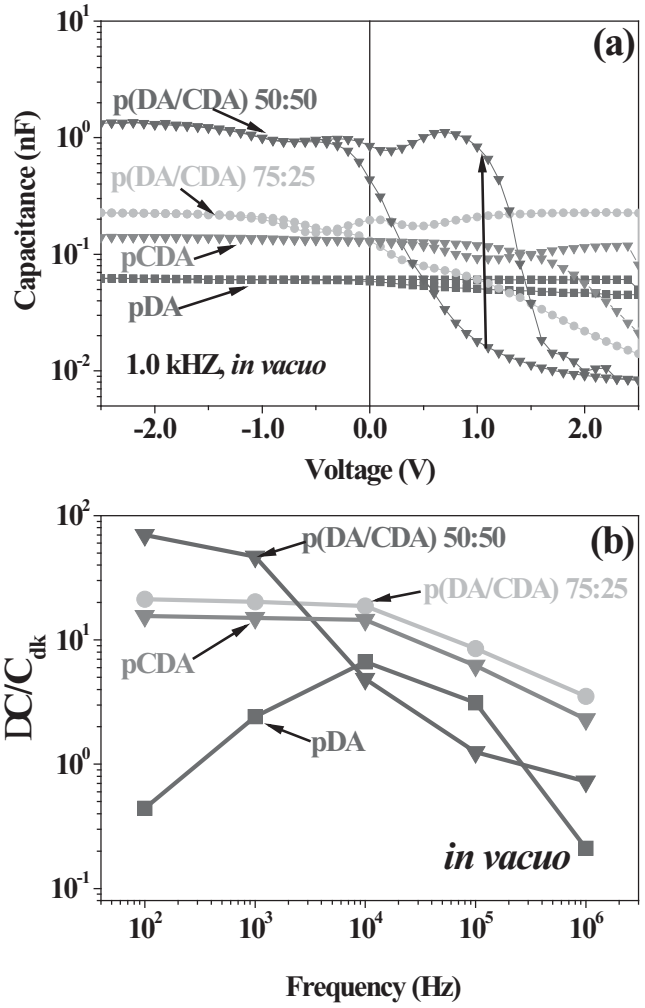

Figure 11. In vacuo: a) Typical photo-assisted C-V data collected at 1 kHz on pDA, pCDA and p(DA/CDA)-based MIS devices. b) Photo-capacitance $\Delta C/C_{dk}$ yield as resulting from photo-assisted C-V measurements at different frequencies of the AC voltage signal.

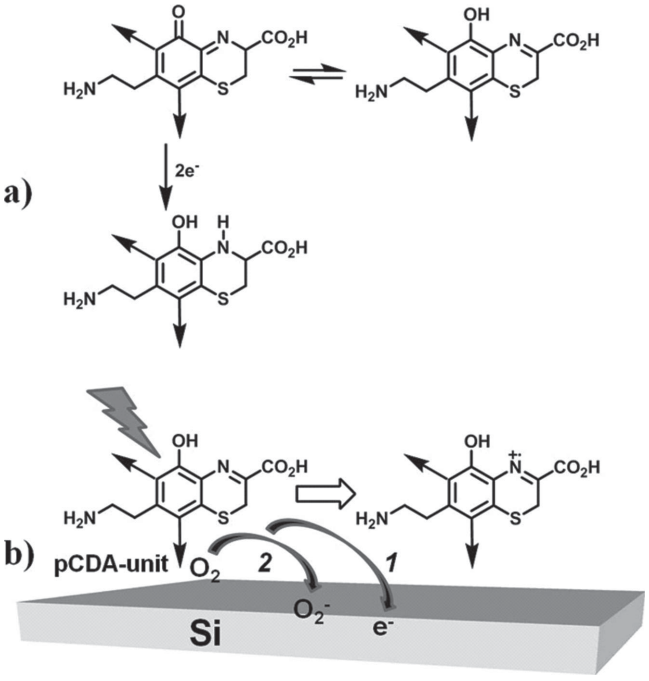

Figure 12. a) Representation of the doping effect mechanisms as a consequence of the presence of different oxidation states of benzothiazine units interacting with pDA. b) Hypothesized pCDA mechanisms excitation induced by visible light promoting the enhancement of photo sensitizing effect of MIS devices in air (path 1) and in vacuo (path 2).

and benzothiazine to the reduced dihydrobenzothiazine forms (**Figure 12**, Scheme (a)), which may interact with the molecular components of pDA, substantially altering their π-electron properties. However, pCDA-related units exhibit a relevant increase of dielectric permittivity (i.e. a high dielectric constant) while keeping the impedance spectra typically encountered in biological materials.[44]

The observed air/vacuum differences would suggest a possible involvement of reactive oxygen species. Based on the known behavior of photoexcited pheomelanins, it would be expected that irradiation of pCDA in air results in electron transfer from the oxidizable benzothiazine units to molecular oxygen (Scheme (b) in Figure 12, path 1), giving rise to the production of superoxide which in turn can inject electrons into the silicon substrate.[32] A direct injection of electrons from photoexcited pCDA units to the silicon substrate (Scheme (b) in Figure 12, path 2) may also be envisaged as a competitive route of electron transfer, likely the dominant one in vacuum. Upon exposure to visible light, pCDA-related units both in MIM and MIS devices elicit an enhanced photo-capacitive response, which may likely reflect the lower photoionization threshold of pheomelanin units (benzothiazines and benzothiazoles) with respect to eumelanin units (5,6-dihydroxyindoles, catechols).

A light-induced generation of photocarriers is more efficient in copolymers, probably due to the increased optical absorption cross section as well as to the presence of the surface dipole (see Figure 10c). *In fact, t*he dipole adds a surface potential able to promoting/increase the injection of the photocarrier from the gold electrode toward the pSi active layer, therefore enhancing the device photoresponse.[48–50] It is worth mentioning, in this connection, the peculiar role of CDA in enhancing the optoelectronic response in term of photocapacitive yield in a wide frequency range (up to 100 kHZ) in MIM and MIS devices as well as its photocarrier ability to follow an AC voltage signal frequency.

4. Conclusions

In this paper we developed an innovative bio-inspired material combining the features of pDA with the characteristic photochemical responsiveness of pheomelanin of red human hair. The new material exhibits remarkable impedance properties closer to those of biological materials rather than of poly-electrolytes, and a marked photocapacitive behavior, finely tunable through the feed ratio of DA and CDA monomers. The incorporation of CDA-derived units resulted in a one order of magnitude enhancement of the photo-impedance of pDA to the white light in a wide frequency range of the AC voltage signal. The

effect of CDA can be attributed to the generation of cyclized benzothiazine and benzothiazole active moieties during oxidative polymerization. Such units can be efficiently photoexcited by visible light above the low energy photoionization threshold thus ejecting electrons into the silicon substrate. Interestingly, the photo-ejected charges are also pushed towards the silicon surface due to the presence of the surface dipole. The enhanced pDA photoresponse following tailoring via pheomelanin-type structures suggests a possible implementation of novel bio-inspired photocapacitive sensors with a chemically tunable response to visible light.

The similarity of the novel copolymer to human Substantia Nigra neuromelanin[36] paves the way for disclosing the neuromelanin response mechanisms to continuous or AC electrical stimuli. In this sense, the described approach could be foreseen as an alternative tool for shedding light, for example, on the modification of electrical signal transmission of diseased neuromelanin-based biological items as well as for probing the effectiveness of tissue repairing processes.

5. Experimental Section

Synthesis and Characterization of CDA, pDA and p(DA/CDA) Melanins: 5-S-cysteinyldopamine (CDA) was prepared on gram scale by the method previously described for the synthesis of 5-S-cysteinyldopa.[51,52] Identity and purity of the compound was secured by comparison with literature data.[34] pDA and pCDA were prepared by autoxidation of DA or CDA in 0.05 M NH_3 buffer, pH 8.5 at 10 mM final concentration according to Bernsmann *et al.*[53] After 24 hours under vigorous stirring, the reaction mixture was acidified to pH 2 with 3M HCl and the pigment that separated was collected by centrifugation at 7000 rpm at 4 °C, washed 3 times with slightly acidic water and lyophilized for 12 hours. pDA and pCDA w/w yields were 48% and 35%, respectively. p(DA/CDA) copolymers with different feed ratios of the two monomers (75:25 or 50:50) were synthesized following the procedures described above using the starting monomers at 10 mM overall concentration. The w/w yield of 50:50 and 75:25 p(DA/CDA) was 28% and 36%, respectively. For the spectrophotometric analysis the oxidation mixtures were diluted 1:50 v/v in water at 8 hrs reaction time and the spectra were taken at room temperature. Sample analysis by chemical degradation was carried out as described[54] Briefly, the melanin samples (5 mg) were suspended in 1 M NaOH containing 1.5% H_2O_2 (1 mL) and kept under stirring in air. After 18 h, the mixture was acidified to pH 2 with 0.2 M HCl and analyzed by HPLC. Analyses of melanin markers were performed on an HPLC instrument equipped with UV-visible detector, set at 254 and 280 nm. A Synergi Hydro-RP80A column (250 × 4.60 mm, 4 μm) was used, with 1% formic acid taken to pH 2.8 with sodium hydroxide/methanol 97:3 (v/v) as the eluant, at a flow rate of 0.7 ml/min. All experiments were run in triplicate, and HPLC analyses was run in triplicate for each experiment. Solid state ^{13}C CP-MAS NMR spectra were collected at 100.47 MHz on a Bruker Avance II 400 spectrometer, equipped with a Bruker 4 mm MAS probe. The samples were packed into 4 mm zirconia rotors and spun at 8 kHz. Spectra were acquired with a 1H $\pi/2$ pulse width of 3.4 s, a relaxation delay of 4 s and a CP contact time of 2 ms, averaging 10,000 scans

pDA, p(DA/CDA), pCDA Layer Deposition: ITO/glass and pSi support were treated by dielectric barrier discharge plasmas as described elsewhere before polymer layer deposition.[18,19] Synthetic melanin layers were casted from solutions on ITO/glass and spin coated on pSi (1500 RPM) substrates. The layer thicknesses were measured by an Alphastep profiliometer. The measured thickness were 400 nm and 30 nm for the casted and spin coated layers, respectively. The solution were obtained by dissolving 70 mg of sample in water (0.5 mL) and 26% aq. ammonia solution (1 mL). Afterwards, the solutions were stirred and sonicated for 1 h, centrifuged at 3500 rpm for 20 min, then filtered with 45 μm PTFE filter before layer deposition. The films were dried under vacuum (2×10^{-3} mbar) for one day.

MIM and MIS Device Fabrication: A set of metal-insulator-metal (MIM) and metal-insulator-semiconductor (MIS) devices were tailored by thermal evaporating a series of Au dots by using a proper metallic shadow mask at room temperature (Ø = 500 μm, 150 nm thick), on structure consisting of pDA, p(DA/CDA) 75:25, p(DA/CDA) 50:50, and pCDA on ITO/glass for the MIM device (Figure 5a) and on pSi for the MIS device definition ($N_a(pSi) = 10^{16}cm^{-3}$, R(pSi) = 10 ÷ 50 Ω, Figure 5b). The ohmic back contact on pSi was obtained by painting InGa conductive past on the rough back surface of the structure. It should be emphasized that, for statistical purposes, all the measurements were collected for each polymer based device on several top contact pads built upon the pDa or p(DA/CDA) on ITO/glass or on silicon structures.

Device Characterizations: Outlook: The full set of electrical measurements on pDA and p(DA/CDA) – based MIM and MIS devices where performed under dark and white light illumination in air, at a relative humidity degree of 50%. Only for MIS devices, all characterizations have been replicated under vacuum too ($p = 4 \times 10^{-5}$ mbar). The Impedance vs frequency (Z vs. f), Capacitance (C) and Conductance (G) vs voltage V (C -.V, G – V) hysteresis loops, photo-capacitance (C_{ph} – V) and photo-capacitance C_{ph} on-off effects (C_{ph} vs. t) have been read out by using a Novocontrol Impedance Analyzer. The MIM and MIS device characterizations under white light illumination have been performed by using a 35 W continuous white light lamp as the illumination source.

MIM Device Characterizations: Z vs. f measurements have been performed at zero DC bias in the frequency range 1.0 Hz-1.0 MHz and applying an AC voltage V_{AC} = 5.0 mV. The data have been used for determining of the real (ε') and imaginary (ε'') part of the dielectric permittivity and of the loss factor tan $\delta = \varepsilon''/\varepsilon'$ following the well know theory on dielectric permittivity.[45] On-off photo-capacitance effect at selected values of the AC voltage frequencies (100 Hz, 1 kHz, 10 kHz) was read out on MIM devices and at zero DC bias by switching on/off the continuous white light source at an interval of Δt = 50 s.

MIS Device Characterizations: The C-V hysteresis loops were read out under dark and white light in the frequency range 100 Hz – 1.0 MHz of the sine wave voltage signal with a signal amplitude V_{AC} = 50 mV, superimposed to the continuous voltage V_{DC} varying in the range ± VL = 3.0 V (from now ahead terming VL as voltage loop amplitude) and applied between the top and bottom contacts. The voltage was first swept from the MIS depletion to the accumulation regime (i.e. from V_L to -V_L for the MIS structure on pSi) and vice versa for the backward sweep. (see also S.I. for all theoretical aspects on MIS device functioning regimes under an applied bias). The flat band capacitance (C_{FB}) and conductance (G_{FB}) of the pDA-based MIS devices are used as the reference values for the estimate of the relative variation of the flat band capacitance $\Delta C_{FB}/C_{FB}$(DA) where $\Delta C_{FB} = C_{FB}$(pDA/DA)- ΔC_{FB}(pDA), and conductance $\Delta G_{FB}/G_{FB}$(DA) where $\Delta G_{FB} = G_{FB}$(pDA/DA)- ΔG_{FB}(pDA). The C–V photo-capacitance effect of the MIS device was readout both in air and under vacuum. (see Figure S6 and S7) The experiments were accomplished by sweeping first the MIS device from accumulation to the depletion conditions (i.e. from V_L = –2.5 V to V_L = + 2.5 V), then the white light source was switched on at V_L = +2.5 V and the photo-capacitance read out was collected during the backward voltage sweep (i.e. sweeping MIS device from depletion to accumulation). The selected AC voltage signal frequencies have been fixed at 100 kHZ, 10 kHz, 1.0 kHZ and 100 Hz. A better estimate of the photo-capacitance yield was desumed by the photo-capacitance C_{ph} on–off effect vs time t (C_{ph} vs. t). The (C_{ph} vs. t, see data in S.I.) behaviour has been detected at the elicited selected AC voltage signal frequencies, by illuminating the MIS device under depletion condition (i.e. by biasing the device under a fixed positive value of the continuous DC voltage V_{DC} = + 2.5) for a certain interval of time (Δt = 50 s). The chosen V_{DC} value corresponds to the starting voltage of the backward step under white light in the elicited C_{ph} vs. V photo-capacitance experiments. The photo-yields have been

calculated as $\Delta C/C_{dk,}$ where C_{dk} is the capacitance value under dark and $\Delta C = C_{ph} - C_{dk}$.

Supporting Information

Supporting Information is available from the Wiley Online Library or from the author.

Acknowledgements

This work was supported in part by grants from Italian MIUR (PRIN 2010–2011 (2010PFLRJR project-PROxi project), and was carried out in the frame of the EuMelaNet activities.

Received: April 29, 2014
Revised: July 15, 2014
Published online:September 8, 2014

[1] C.-H. Lin, C. W. Liu, *Sensors* **2010**, *10*, 8797.
[2] J. Grosvalet, C. Jund, *IEEE Trans. Electron Devices* **1967**, *14*, 777.
[3] B. C. Paul, M. Satyam, A. Selvarajan, *IEEE Trans. Electron Devices* **1999**, *46*, 324.
[4] M. Shah, K. S. Karimov, M. H. Sayyad, *Semicond. Sci. Technol.* **2010**, *25*, 075014.
[5] P. Chakrabarti, B. R. Abraham, A. Dhingra, A. Das, B. S. Sharan, V. Maheshwari, *IEEE Trans. Electron Devices* **1992**, *39*, 507.
[6] D. M. Kim, H. C. Kim, H. T. Kim, *IEEE Trans. Electron Devices* **2002**, *49*, 526.
[7] E. Ahlstrom, W. G. Matthei, W. W. Gärtner, *Rev. Sci. Instrum.* **1959**, *30*, 592.
[8] T. Yang, Y. Xuan, D. Zemlyanov, T. Shen, Y. Q. Wu, J. M. Woodall, P. D. Ye, F. S. Aguirre-Tostado, M. Milojevic, S. McDonnell, R. M. Wallace, *Appl. Phys. Lett.* **2007**, *91*, 142122.
[9] D. Čiplys, V. S. Chivukula, A. Sereika, R. Rimeika, M. S. Shur, X. Hu, R. Gaska, *Electron. Lett.* **2009**, *45*, 653.
[10] V. Chivukula, D. Ciplys, A. Sereika, M. Shur, J. Yang, R. Gaska, *Appl. Phys. Lett.* **2010**, *96*, 163504.
[11] M. W. Cowens, M. M. Blouke, T. Fairchild, J. A. Westphal, *Appl. Opt.* **1980**, *19*, 3727.
[12] J. W. Levell, M. E. Giardini, I. D. W. Samuel, *Opt. Express* **2010**, *18*, 3219.
[13] S. Ito, K. Wakamatsu, M. d'Ischia, A. Napolitano, A. Pezzella, In *Melanins and Melanosomes: Biosynthesis, Biogenesis, Physiological, and Pathological Functions*, (Eds: J. Borovanský, P. A. Riley) Wiley-VCH, Weinheim, Germany, **2011**, p. 167.
[14] P. Meredith, T. Sarna, *Pigment Cell Res.* **2006**, *19*, 572.
[15] M. d'Ischia, K. Wakamatsu, A. Napolitano, S. Briganti, J.-C. Garcia-Borron, D. Kovacs, P. Meredith, A. Pezzella, M. Picardo, T. Sarna, J. D. Simon, S. Ito, *Pigment Cell Melanoma Res.* **2013**, *26*, 616.
[16] P. Meredith, C. J. Bettinger, M. Irimia-Vladu, A. B. Mostert, P. E. Schwenn, *Rep. Prog. Phys.* **2013**, *76*, 034501.
[17] M. d'Ischia, A. Napolitano, A. Pezzella, P. Meredith, T. Sarna, *Angew. Chem. Int. Ed. Engl.* **2009**, *48*, 3914.
[18] M. Ambrico, A. Cardone, T. Ligonzo, V. Augelli, P. F. Ambrico, S. Cicco, G. M. Farinola, M. Filannino, G. Perna, V. Capozzi, *Org. Electron.* **2010**, *11*, 1809.
[19] M. Ambrico, P. F. Ambrico, A. Cardone, T. Ligonzo, S. R. Cicco, R. Di Mundo, V. Augelli, G. M. Farinola, R. Di Mundo, *Adv. Mater.* **2011**, *23*, 3332.
[20] J. McGinness, P. Corry, P. Proctor, *Science* **1974**, *183*, 853.
[21] H. J. Nam, J. Cha, S. H. Lee, W. J. Yoo, D.-Y. Jung, *Chem. Commun.* **2014**, *50*, 1458.
[22] J. H. Waite, *Nat. Mater.* **2008**, *7*, 8.
[23] V. Ball, D. Frari, M. Michel, M. J. Buehler, V. Toniazzo, M. K. Singh, J. Gracio, D. Ruch, *Bionanoscience* **2011**, *2*, 16.
[24] Y. Liu, K. Ai, L. Lu, *Chem. Rev.* **2014**, *114*, 5057.
[25] D. R. Dreyer, D. J. Miller, B. D. Freeman, D. R. Paul, C. W. Bielawski, *Chem. Sci.* **2013**, *4*, 3796.
[26] H. Lee, S. M. Dellatore, W. M. Miller, P. B. Messersmith, *Science* **2007**, *318*, 426.
[27] M. Ambrico, P. F. Ambrico, A. Cardone, N. F. Della Vecchia, T. Ligonzo, S. R. Cicco, M. M. Talamo, A. Napolitano, V. Augelli, G. M. Farinola, M. d'Ischia, *J. Mater. Chem. C* **2013**, *1*, 1018.
[28] S. Hong, Y. S. Na, S. Choi, I. T. Song, W. Y. Kim, H. Lee, *Adv. Funct. Mater.* **2012**, *22*, 4711.
[29] N. F. Della Vecchia, R. Avolio, M. Alfè, M. E. Errico, A. Napolitano, M. d'Ischia, *Adv. Funct. Mater.* **2013**, *23*, 1331.
[30] J. Liebscher, R. Mrówczyński, H. A. Scheidt, C. Filip, N. D. Hădade, R. Turcu, A. Bende, S. Beck, *Langmuir* **2013**, *29*, 10539.
[31] C.-T. Chen, V. Ball, J. J. de Almeida Gracio, M. K. Singh, V. Toniazzo, D. Ruch, M. J. Buehler, *ACS Nano* **2013**, *7*, 1524.
[32] T. Ye, L. Hong, J. Garguilo, A. Pawlak, G. S. Edwards, R. J. Nemanich, T. Sarna, J. D. Simon, *Photochem. Photobiol.* **2006**, *82*, 733.
[33] S. P. Nighswander-Rempel, *Biopolymers* **2006**, *82*, 631.
[34] F. Zhang, G. Dryhurst, *J. Med. Chem.* **1994**, *37*, 1084.
[35] X. Shen, G. Dryhurst, *Tetrahedron* **2001**, *57*, 393.
[36] K. Wakamatsu, K. Fujikawa, F. A. Zucca, L. Zecca, S. Ito, *J. Neurochem.* **2003**, *86*, 1015.
[37] A. Napolitano, L. Panzella, L. Leone, M. D'Ischia, *Acc. Chem. Res.* **2013**, *46*, 519.
[38] A. Napolitano, M. De Lucia, L. Panzella, M. d'Ischia, *Photochem. Photobiol.* **2008**, *84*, 593.
[39] R. A. Zangmeister, T. A. Morris, M. J. Tarlov, *Langmuir* **2013**, *29*, 8619.
[40] U. Kolczyriski-Szafraniec, B. Bilinska, *Curr. Top. Biophys.* **1992**, *16*, 77.
[41] G. Greco, L. Panzella, L. Verotta, M. d'Ischia, A. Napolitano, *J. Nat. Prod.* **2011**, *74*, 675.
[42] L. Panzella, L. Leone, G. Greco, G. Vitiello, G. D'Errico, A. Napolitano, M. d'Ischia, *Pigment Cell Melanoma Res.* **2014**, *27*, 244.
[43] G. Schwarz, *J. Phys. Chem.* **1962**, *66*, 2636.
[44] H. P. Schwan, In *Advances in Biological and Medical Physics*, Vol. *5*, (Eds. J. H. Lawrence, C. A. Tobias), Academic Press Inc., New York, **1957**, pp. 147–209.
[45] In *Impedance Spectroscopy: Theory, Experiment, and Applications*, (Eds: E. Barsoukov, J. R. Macdonald), J. Wiley & Sons, Inc., Hoboken, New Jersey, **2005**.
[46] E. H. Nicollian, J. R. Brews, *MOS (Metal Oxide Semiconductor) Physics and Technology*, Wiley, New York, **1981**.
[47] M. Ambrico, P. F. Ambrico, T. Ligonzo, A. Cardone, S. R. Cicco, A. Lavizzera, V. Augelli, G. M. Farinola, *Appl. Phys. Lett.* **2012**, *100*, 253702.
[48] I. Visoly-Fisher, A. Sitt, M. Wahab, D. Cahen, *Chemphyschem* **2005**, *6*, 277.
[49] H. Haick, M. Ambrico, T. Ligonzo, D. Cahen, *Adv. Mater.* **2004**, *16*, 2145.
[50] Y. Zhang, M. Wang, S. D. Collins, H. Zhou, H. Phan, C. Proctor, A. Mikhailovsky, F. Wudl, T.-Q. Nguyen, *Angew. Chem. Int. Ed. Engl.* **2014**, *53*, 244.
[51] F. Chioccara, E. Novellino, *Synth. Commun.* **1986**, *16*, 967.
[52] C. Aureli, T. Cassano, A. Masci, A. Francioso, S. Martire, A. Cocciolo, S. Chichiarelli, A. Romano, S. Gaetani, P. Mancini, M. Fontana, M. d'Erme, L. Mosca, *J. Neurosci. Res.* **2014**, *92*, 347.
[53] F. Bernsmann, A. Ponche, C. Ringwald, J. Hemmerlé, J. Raya, B. Bechinger, J. Voegel, P. Schaaf, V. Ball, *J. Phys. Chem. C* **2009**, *113*, 8234.
[54] L. Panzella, P. Manini, G. Monfrecola, M. d'Ischia, A. Napolitano, *Pigment Cell Res.* **2007**, *20*, 128.